Numerical investigation of the effect of crosswind on cyclists

D.M. Fintelman[1], H. Hemida[2], M. Sterling[2] and F-X Li[1]

[1]School of Sport, Excercise and Rehabitation Sciences, University of Birmingham, UK.

[2]School of Civil Engineering, University of Brimingham, UK.

DMF144@bham.ac.uk

Abstract

The aim of the study was to investigate the effect of crosswind on the aerodynamic responses of cyclists. The Reynolds Averaged Navier Stokes (RANS) SST k-ω model and k-ε turbulence models were employed. The geometry was a full scale model of a cyclist on a bicycle. The Reynolds number was 8.9×10^5, based on the effective wind velocity and height of the cyclist from the floor. A good agreement (RMSE =0.12) has been found between the simulation results and the experimental data. The aerodynamic force coefficients at different yaw angles have been obtained and the main feature of the flow around the cyclist determined. The results of this study will help to improve the understanding of the aerodynamic behaviour of cyclists in crosswind.

1 Introduction

Crosswinds can have an impact on the performance, stability and safety of a cyclist. To the best of the author's knowledge no studies have investigated the effect of crosswind on the aerodynamic behaviour of cyclists at yaw angles > 30 ° (i.e. the angle of the wind with the cyclists direction of travel as shown in Fig. 1) despite the several occurrences of fatal accidents due to crosswinds (Department of Transport, 2012). To improve the safety of cyclists and equipment, it is crucial to understand the flow field around cyclists and to calculate the corresponding aerodynamic forces. There are different methods which can be used to investigate the flow pattern around cyclists and one of these is numerical modelling, i.e., Computational Fluid Dynamic (CFD) simulations. CFD analysis gives comprehensive information compared to analytical and experimental fluid dynamics, where information is dependent on the position of the measurement instrument. Conversely, only a limited number of CFD based studies in cycling are published (Hanna, 2002; Lukes et al., 2004; Defraeye et al., 2010; Griffith et al., 2012). Except a study on the effect of disk wheels in full side wind (Hanna, 2002), all current CFD studies are focused on windless environmental conditions. Since it is appreciated by road safety specialists, road designers and bicycle developers that worse case conditions can occur, side wind analysis at crosswind yaw angles > 30 ° is essential. However, a comprehensive study about the effect of crosswind on bicycle and cyclist is lacking in the literature. Hence, the aim of this CFD study is to investigate the effect of crosswind on cyclists at different crosswind yaw angles.

2 Method

The flow around a cyclist on a bicycle is computed for different crosswind angles ranging between 0 to 90°. The flow field around a cyclist is obtained with two different Reynolds Averaged Navier

Stokes (RANS) turbulence models: the two-equation SST k-ω and k-ε models. These models are commonly used in crosswind vehicle studies. The method is validated with full-scale wind tunnel experiments of a mannequin on a bicycle (Fig 1a). In order to simulate realistic flow conditions, the geometry of the mannequin on the bicycle of the wind tunnel experiments is used as shown in Fig. 1b. The geometry has a high level of complexity. All main components are included in the computational model, whilst smaller features have been excluded such as the bicycle cables, spokes, chain and brakes, as these small details will consume many grid cells. The cyclist has been positioned with straight arms, the hands on the dropped handlebars and in a torso angle position of 24° with respect to the ground.

The computational domain is shown in Fig. 2a, where H (1.35m) represents the height of the cyclists. The bicycle has been placed on the floor of the computational domain as shown in Fig. 2a. A generalized computational domain has been used in all simulations, regardless of the crosswind conditions. The domain has a length, width and height of 21H, 21H and 5.2H respectively. The front wheel of the bicycle has been positioned 4.6H from the front and side inlet to prevent effects of the bicycle on the pressure inlet. A refinement box has been defined around the bicycle and cyclist to refine the mesh in the region close to geometry. The length, width and height of the refinement box are respectively 5.7H, 5.1H and 1.3H. Three different meshes are created with different number of nodes. The coarse, medium and fine mesh consist of $7.3\text{x}10^6$, $13.1\text{x}10^6$ and $17.9\text{x}10^6$ nodes, respectively. An example of the surface mesh is shown in Fig. 2b. For the fine mesh, the dimensionless normal wall distance is 25.2.

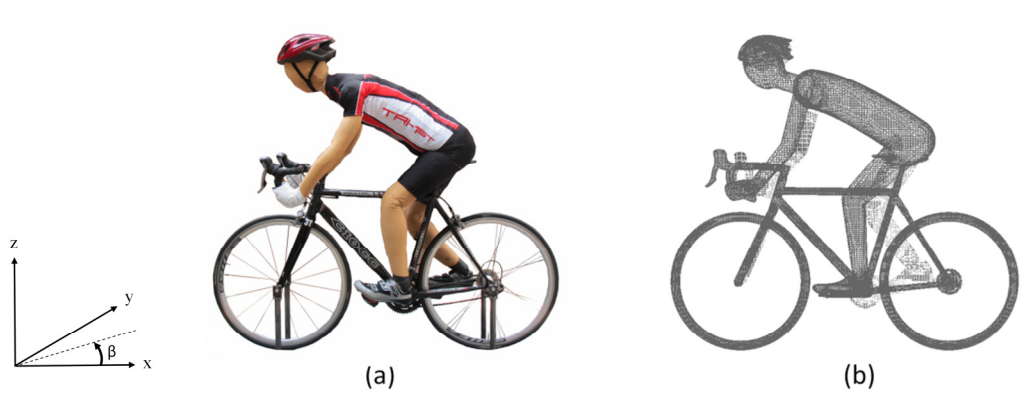

Figure 1: (a) Bicycle with mannequin used in the wind tunnel experiments and (b) geometry of bicycle with cyclist in the simulations.

The initial conditions of the simulations are chosen to closely reassemble the wind tunnel experiments. A turbulence intensity (i.e. standard deviation divided by the mean wind velocity) of 0.67 % is used at the inlet of the domain. Different yaw angles, β, have been analysed. Simulations have been carried out for yaw angles between 0° and 90°, with increments of 15°. Similar to the wind tunnel experiments, a uniform effective velocity, U_∞, of 9.91 m/s is applied for all different yaw angles, β. The velocity in the main inlet direction, U_x, and in the crosswind inlet direction , U_y, is calculated by:

$$U_x = U_\infty \cos(\beta)\ , U_y = U_\infty \sin(\beta). \quad (1)$$

A Reynolds number of $8.9\text{x}10^5$ is used based on the effective wind velocity and the height of the cyclists from the ground. To enable to compare the results with the wind tunnel results, stationary ground and wheels have been simulated. No slip-boundary conditions have been given to the surface of the model and the ground. Free slip velocity boundary conditions are applied on the sides and upper walls.

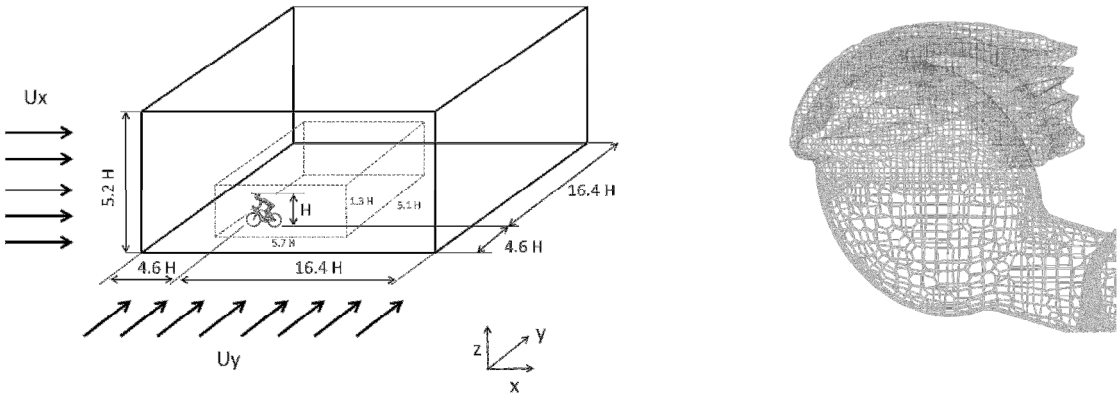

(a) (b)

Figure 2: (a) Computational domain, (b) surface mesh of cyclist

All simulations have been performed in OpenFOAM. The steady state SIMPLE algorithm is implemented in the simulations to couple the pressure and the velocity. In all simulations an incompressible flow is assumed. The simulations have run on 32 processors on the BlueBEAR (Birmingham Environment for Academic Research) in parallel.

3 Results and discussion

In this section, the mesh dependency, the aerodynamic coefficients and flow structures around the cyclists at different yaw angles is explored. The flow structures are visualised with Ensight. All results are from the fine RANS simulations unless otherwise stated.

Mesh dependency

To attain a mesh independent mesh, the aerodynamic forces of the different meshes are compared. The aerodynamic forces are usually expressed by force coefficients. The drag force coefficient C_D, side force coefficient C_S and lift force coefficient C_L, are defined by:

$$C_D = \frac{F_D}{0.5A\rho {U_\infty}^2}, C_S = \frac{F_S}{0.5A\rho {U_\infty}^2}, \; C_L = \frac{F_L}{0.5A\rho {U_\infty}^2}, \tag{2}$$

where ρ the air density (kg/m^3), A the total frontal area of the cyclist and bicycle at 0° yaw angle (0.55 m^2), U_∞ the effective flow velocity (m/s), and F_D, F_S and F_L respectively the drag force, side force and lift force (N). The aerodynamic force coefficients as function of grid size are shown in Table 1. A small error difference of 4.3 % is obtained in the drag force coefficient results from the medium and fine mesh.

Table 1: RANS aerodynamic force coefficients for RANS k-ε simulations at β=0°. Error percentage of the simulation results compared to the fine simulation results and the experimental data. The error is defined as: Value- Reference value / Reference value.

		C_D	C_S	C_L
Coarse	Value	0.638	0.000	0.102
	% Error Fine	15.1	-100.0	14.6
	% Error Exp.	4.4	-100.0	-30.6
Medium	Value	0.578	0.040	0.075
	% Error Fine	4.3	-14.9	-15.7
	% Error Exp.	-5.4	-14.9	-49.0
Fine	Value	0.554	0.047	0.089
	% Error Exp.	-9.3	0.0	39.5
Experiments	Value	0.611	0.047	0.147

In addition, the surface pressure of the cyclist at a height of 0.7H is obtained from the coarse, medium and fine mesh as shown in Fig. 3. The pressure distribution is expressed in terms of the local pressure coefficient C_p. The C_p is defined as:

$$C_p = \frac{p - p_\infty}{0.5\rho {U_\infty}^2}, \quad (3)$$

where p is the local pressure, p_∞ the free stream pressure and ρ the air density. The good agreement (RMSE = 0.12) between the results obtained from the fine and medium meshes suggest that the fine mesh simulation accurately predict the flow and no further mesh refinement is needed.

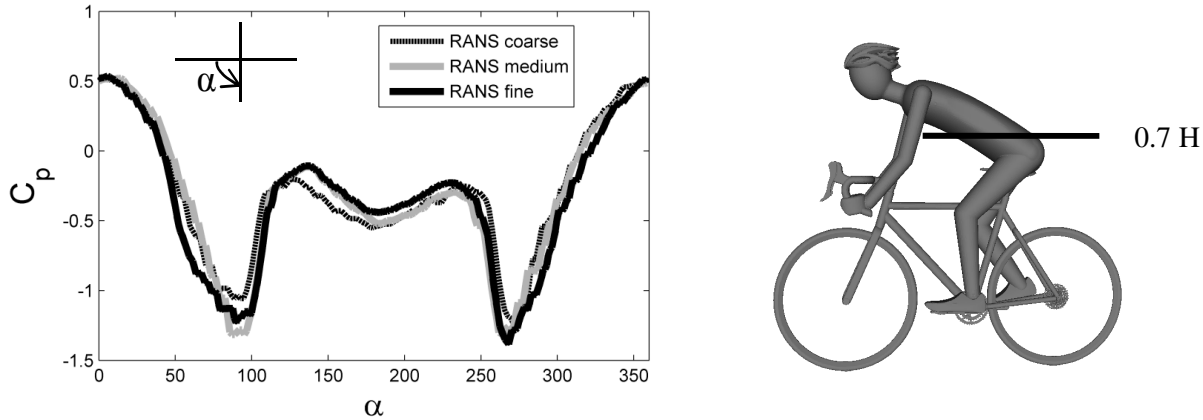

Figure 3: Pressure distribution around the surface of the main body of the cyclist obtained from the coarse, medium and fine mesh RANS k-ε simulations at β=0°.

Aerodynamic force coefficients

The aerodynamic force coefficient at different crosswind angles is shown in Fig. 4. At full head wind, i.e. $\beta = 0°$, the drag force coefficient is around 0.55. A peak drag coefficient is found at $\beta = 15°$, after which the drag force coefficient constantly decreases. The increase in drag force from $\beta = 0°$ to $\beta = 15°$ is caused by the increase of frontal area and the less aerodynamic shape of the cyclist. The side force coefficient gradually increases with yaw angle. The lift forces are compared to the side forces up to 37 times smaller and therefore excluded from consideration.

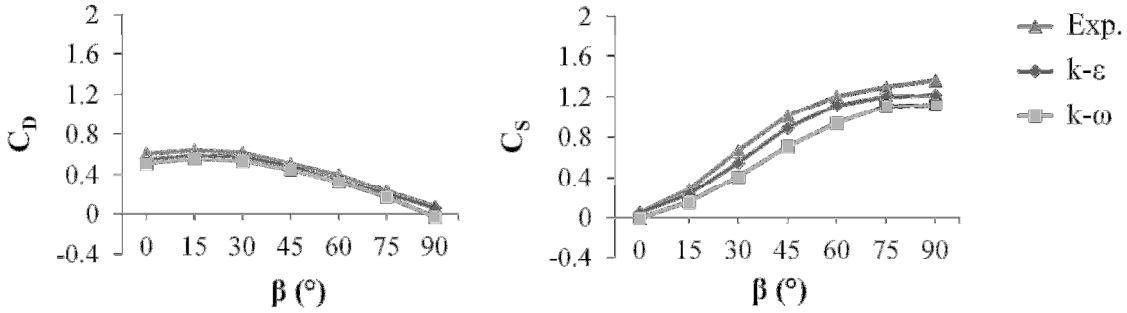

Figure 4: Aerodynamic force as function of yaw angle with mannequin in 24° torso angle position of the experiments and the k-ε and k-ω turbulence models.

The error of the CFD results with the wind tunnel results is expressed as a relative percentage difference:

$$Pct = \frac{AC_{i,CFD} - AC_{i,wt}}{AC_{i,wt}}, \quad (4)$$

where $AC_{i,CFD}$ is the aerodynamic force coefficients of the CFD simulations in all i directions and $AC_{i,wt}$ the measured wind tunnel force coefficients in all directions. The results of the comparison of the force coefficients of the CFD simulations and the wind tunnel experiments are shown in Fig. 5. The smallest difference in simulation results are found with the k-ε model in all analysed force directions. Both two- equation RANS turbulence models slightly underestimate the total drag force and side force coefficient. The average difference percentage in drag for yaw angles $\beta = 0 - 45°$ is -7 % for the k-ε model and -13 % for the k-ω model. The side force differences in the yaw angle range $\beta = 45 - 90°$ are -9 % and -21 % for respectively the k-ε and k-ω model.

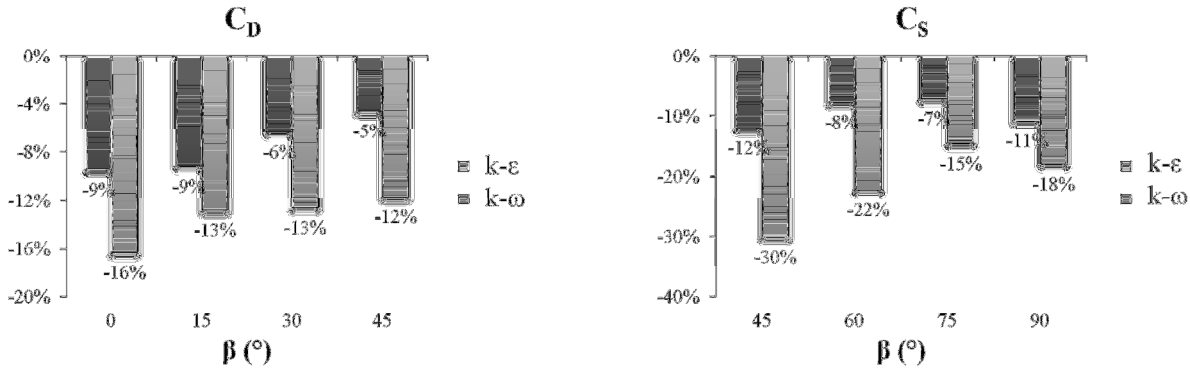

Figure 5: Relative percentage difference aerodynamic drag force and side force coefficient of the RANS k-ε and k-ω simulations.

In the RANS simulation results, a distinction is made between the pressure forces and skin friction forces. The skin friction is caused by the viscous pressure in the boundary layer around the bicycle and cyclist. In the RANS simulations approximately 3 % of the total drag forces contribute to skin drag versus 2 % of the total side forces. This relatively low viscous forces are comparable with that of an isolated cyclist [1] and might be caused by the smooth surface roughness of the cyclist model. It could be therefore expected that the predicted viscous forces in the simulations are higher in the wind tunnel experiments, where the cyclists' surface was not perfectly smooth. However, the total

experimentally recorded drag is only around 10 % higher compared to the simulation results and therefore it is likely that this effect is limited.

Pressure distribution

The pressure distribution over the surface of the geometry in different crosswind angles is shown in Fig. 6. A low pressure area develops at the back of the cyclist by increasing yaw angles, while high pressure regions are developing on the upper lower limbs and the abdomen. At full side wind ($\beta = 90°$), high pressure areas at the wind ward side of the cyclist are present, while low pressure regions develop on the back of the cyclist and the leeward side of the cyclist.

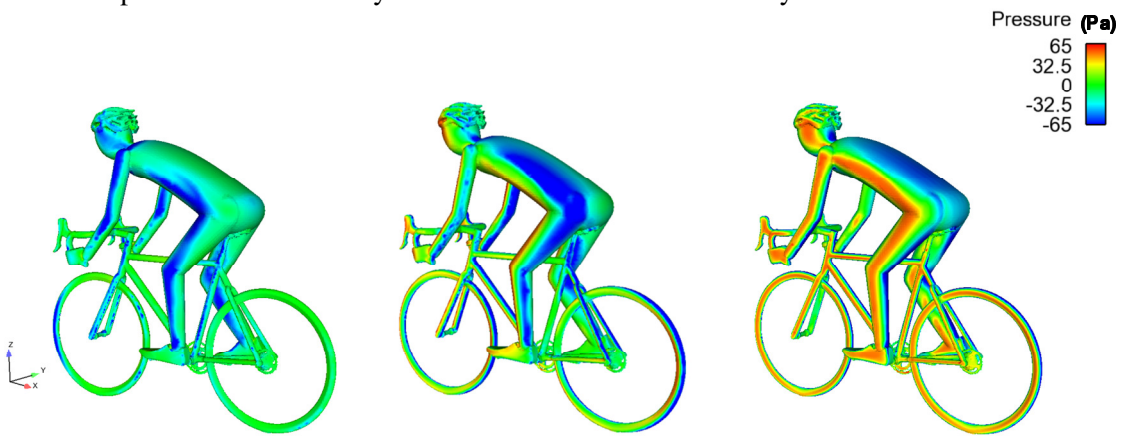

Figure 6: Pressure distribution on the surface of the cyclist in different crosswind yaw angles of the RANS standard *k-ε* turbulence model: (a) β = 0°, (b) β = 45° and (c) β = 90°.

Pressure contour lines

Fig. 7 shows the pressure contour lines on the cyclist in head wind ($\beta = 0°$). The mean stagnation points can be found on the head (S1), the shoulders (S2), the pelvis (S3), the hands (S4) and the ankles of the cyclist (S5). The stagnation points are moving to the wind ward side of the cyclist with increasing yaw angles.

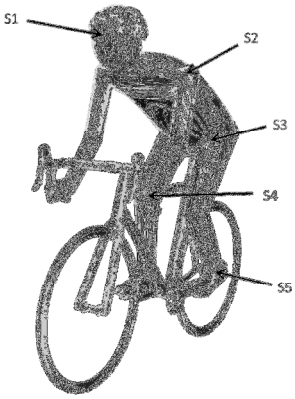

Figure 7: Pressure contour lines on the cyclist surface in case of head wind ($\beta = 0°$) of the RANS standard *k-ε* turbulence model. Mean stagnation points are found on the head (S1), shoulders (S2), pelvis (S3), hands (S4) and ankles (S5) of the cyclist.

Vortex cores analysis

The vortex cores of the flow around the cyclists are found by means of Eigen analysis. This method is based on an algorithm of Sujudi and Haimes (1995). The location of the vortex for two different yaw angles, i.e. 0 and 60°, is shown in Fig. 8. In case of a crosswind yaw angle of β=0°, the helmet, bicycle and legs mainly contribute to the vortex generation in the flow, while the upper body does not create swirl to the flow. With increasing yaw angles, it should be noticed that the vortex cores move from the back of the cyclists towards the side of the cyclist. At large crosswind angles, practically all vortex cores are in the direction of the main flow.

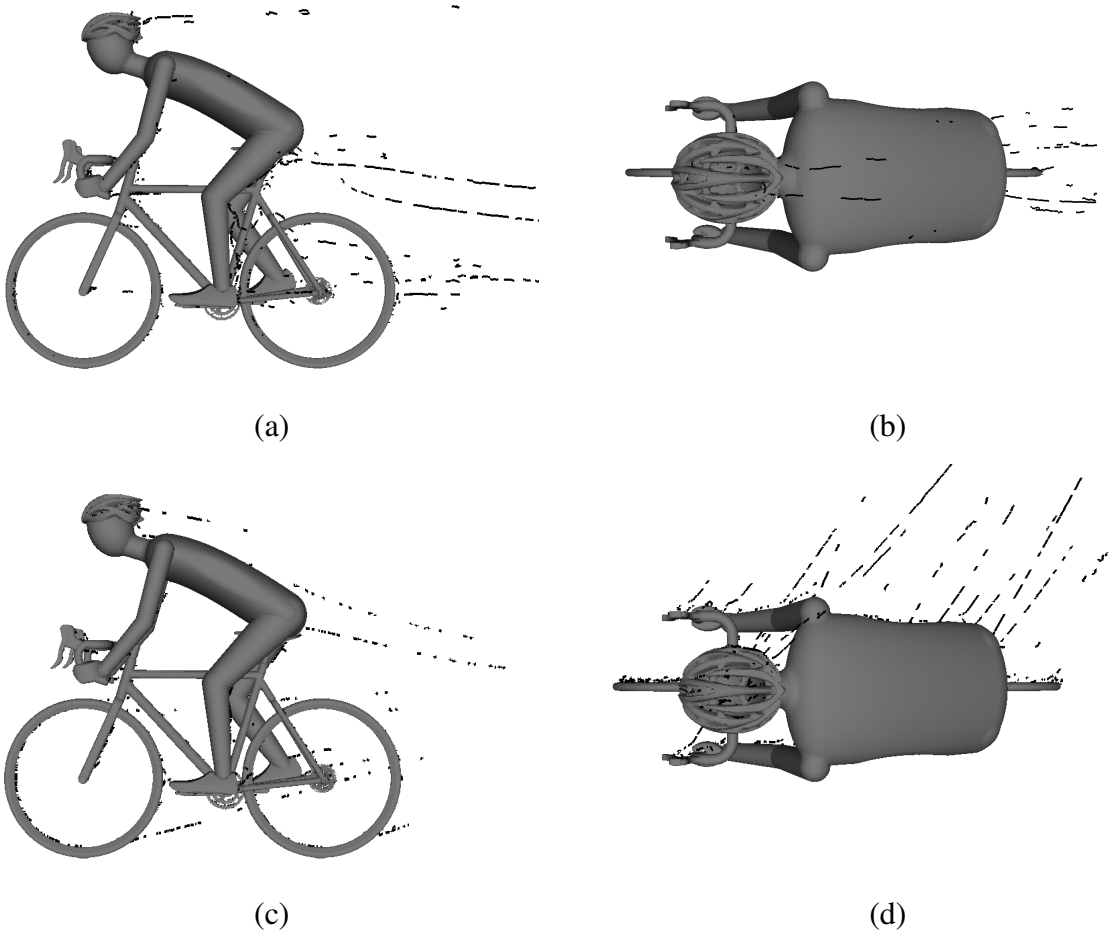

(a) (b)

(c) (d)

Figure 8: Location of the vortex cores in the flow around a cyclists: (a) β=0° side view; (b) β=0° top view; (c) β=60° side view; (d) β=60° top view

Isosurface around cyclist

The isosurface around the cyclists at C_p = -0.240 at different crosswind angles is shown in Fig. 9. The isosurface is mainly attached to the cyclist at this pressure. In the case of 60° side wind yaw angle, besides the cyclists body also a pressure surface is located at the leeward side of the entire bicycle. This flow characteristic is caused by the slender body of the bicycle.

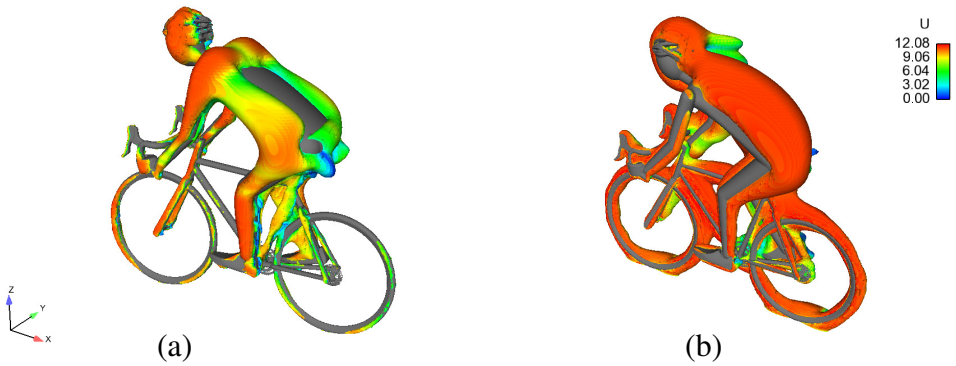

(a) (b)

Figure 9: Isosurface of the time averaged pressure at C_p = -0.240 at different yaw angles; (a) β=0°; (b) β=60°

4 Conclusions

Two RANS simulations have been employed for a cyclist on a bicycle in different crosswinds. The results showed that crosswind has a significant effect on the aerodynamic force coefficients. Good agreement has been found between the trend of the CFD results and the experimental data across a wide range of yaw angles. Both the k-ε and k-ω RANS turbulence models under-predict the aerodynamic forces, likely caused by discrepancies in surface friction. The flow structures have been identified and the aerodynamic coefficients have been obtained. Future research will involve investigating the effect of time varying wind and the implications on the stability of cyclists and improving the CFD model by using time varying solver, large-eddy simulations.

References

Defraeye, T., Blocken, B., Koninckx et al. 2010. Computational fluid dynamics analysis of the cyclist aerodynamics: Performance of different turbulence-modelling and boundary-layer modelling approaches. *Journal of Biomechanics*, **42** (12), 2281-2287.

Great Britain. Department of Transport, 2012. Reported Road Casualties in Great Britain: Main Results 2011, Statistical Release.

Griffith, M., Crouch, T., et al. 2012. Elite Cycling Aerodynamics: Wind Tunnel Experiments and CFD. *In: 18th Australasian Fluid Mechanics Conference*, Launceston, Australia.

Hanna R.K. 2002. Can CFD make a performance difference in sport? *The engineering of sport 4*. Blackwell Science Ltd.

Lukes, R.A., Chin, S.B., et al. 2004. The aerodynamics of mountain bicycles: the role of computational fluid dynamics. *The engineering of sport 5*. International Sports Engineering Association.

Sujudi, D., Haimes, R. 1995. Identification of Swirling Flow in 3-D Vector Fields. Technical Report AIAA-95-1715, American Institute of Aeronautics and Astronautics.